Updated November 2025

Disrupted endothelial cell–cell dynamics in ALK1 and SMAD4 deficiency drive arteriovenous malformations

Authors: David Hardman¹, Olya Oppenheim^{2,3}, Wolfgang Giese^{2,3}, Holger Gerhardt^{2,3}, Miguel O. Bernabeu¹

- 1. Centre for Medical Informatics, Usher Institute, The University of Edinburgh, Edinburgh, UK
- 2. Max-Delbrück-Center for Molecular Medicine (MDC) in the Helmholtz Association, Berlin, Germany
- 3. German Center for Cardiovascular Research (DZHK), Partnersite Berlin, Germany.

Email: david.hardman@ed.ac.uk

Author Contributions: David Hardman: Methodology, Investigation, Software, Verification, Formal analysis, Writing – Original Draft. **Olya Oppenheim:** Methodology, Investigation, Resources, Writing – Original Draft. **Wolfgang Giese:** Methodology, Investigation, Writing – Original Draft. **Holger Gerhardt:** Supervision, Project administration, Writing - Review & Editing. **Miguel O. Bernabeu:** Supervision, Writing - Review & Editing

Competing Interest Statement: No competing interests.

Classification: Major: Cell Biology. Minor: Biophysics and Computational Biology.

Keywords: Arteriovenous malformation; hereditary hemorrhagic telangiectasia; endothelial cell dynamics; ALK1; SMAD4; vascular remodelling; agent-based modelling; collective cell migration

Abstract

1

22

34 35

36 37

38

39

40

41 42

43 44

45

- 2 Arteriovenous malformations (AVMs) are a hallmark of hereditary haemorrhagic
- 3 telangiectasia (HHT) and arise from abnormal vascular remodelling. Although AVM
- 4 formation has been associated with disruptions in the BMP9/10 signalling pathway, the
- 5 distinct contributions of its components remain unclear. Here, we combine in vitro
- 6 mosaic endothelial cell (EC) cultures with agent-based modelling (ABM) to investigate
- 7 how knockdown of the BMP9/10 pathway components ALK1 and SMAD4 alters cell-cell
- 8 interactions and collective vascular organisation.
- 9 Using cell tracking data, we inferred the mechanical interactions between neighbouring
- 10 ECs in 2D monolayers by applying Approximate Bayesian Computation to an ABM of
- cell migration. SMAD4 knockdown increased the motile forces generated by ECs, while
- 12 ALK1 knockdown weakened the ability of cells to push apart and rearrange with their
- 13 neighbours, both resulting in greater mixing and fluidity within the cell layer. When these
- 14 altered interaction profiles were incorporated into an ABM of collective EC dynamics
- during vascular remodelling, they gave rise to distinct AVM-prone phenotypes. SMAD4-
- 16 deficient populations exhibited local blockages as highly polarised cells migrated
- 17 excessively, whereas ALK1-deficient populations disrupted vascular patterning by
- impairing coordinated polarity and neighbour separation, favouring flow reversal.
- 19 Our findings suggest that canonical BMP9/10 pathway defects destabilise the
- 20 biomechanical balance of endothelial interactions, leading to emergent collective
- 21 behaviours that predispose vessels to AVM formation.

Significance Statement

- 23 Arteriovenous malformations (AVMs) are abnormal connections between arteries and
- veins that disrupt blood flow and can cause stroke or life-threatening bleeding. They are
- a hallmark of hereditary haemorrhagic telangiectasia (HHT), a genetic vascular disorder,
- but the cellular events that initiate AVMs remain unclear. Using a combination of
- 27 endothelial cell cultures and computational modelling, we show that loss of two key
- 28 HHT-linked genes, ALK1 and SMAD4, disrupts the coordinated movement and
- 29 interactions of endothelial cells. Although both deficiencies lead to AVM-like behaviours,
- 30 they do so through distinct mechanisms. SMAD4 loss drives excessive collective
- migration, whereas ALK1 loss impairs polarity and neighbour separation. These findings
- provide a mechanistic framework for how genetic defects could contribute to cell-cell dynamics observed in vascular malformations.

Main Text

Note: Not all manuscripts need to follow the standard section order or headings outlined below. Authors are welcome to choose headings and subheadings that best fit their work. Materials and Methods should appear after the Results and Discussion in most cases.

Introduction

Vascular remodelling is essential for shaping functional blood vessels, ensuring efficient haemodynamics and tissue perfusion. When remodelling is disrupted, abnormal vessel

- connections known as arteriovenous malformations (AVMs) can arise, with serious 46 47 clinical consequences. Blood flow¹ and endothelial cell (EC) behaviour play a significant role in this remodelling process, polarising and migrating against the direction flow in 48 response to vessel wall shear stress (WSS)2. 49 50 AVMs are a hallmark of hereditary haemorrhagic telangiectasia (HHT), an inherited
- vascular disorder. Type 2 HHT is caused by loss-of-function mutations in the endothelial 51 52 surface receptor Activin-receptor-like kinase 1 (AVCRL1 encoding ALK1)3. SMAD4 functions downstream of ALK1 in the Bone Morphogenic Protein (BMP) 9/10 pathway 53 and of ALK5 in the Transforming Growth Factor Beta (TGF-β) pathway, and is a shared 54 55 mediator in activin signaling. Mutations in the SMAD4 gene are present in families with Juvenile Polyposis/HHT syndrome. Deletion of both endothelial Alk1 and Smad4 in 56 57 mouse models⁴ have resulted in AVM formation and lethality though the relative effects 58 of ALK1 and SMAD4 on AVM formation and the mechanisms by which they mediate EC 59 behaviour in AVM formation remain poorly understood. While these animal models have been invaluable, they do not allow direct live imaging of AVM initiation within intact 60
- 62 been described in detail in vivo. To determine the influence that inhibiting ALK1 and SMAD4 has on healthy cells, we 63 conducted in vitro experiments with human umbilical venous endothelial cells (HUVEC) 64 65 on mosaic populations combining knockdowns of either ALK1 or SMAD4 with control 66 cells and tracked the dynamics of cell motion over time.

vasculature, meaning that the cell-cell dynamics underlying AVM formation have not yet

- Previous work by Edgar et als applied an agent-based model (ABM) of EC motion and 67 mechanical cell-cell interactions on idealised vascular networks to investigate the 68 69 collective dynamics of cells during vascular remodelling. Distinct regimes of EC force dynamics favourable to AVM creation were identified based upon theoretical forces of 70 71 cell motility, contractility, and adhesion, together with the proportion of cells moving with or against the direction of WSS. A similar modelling approach based on self-propelled 72 73 particles (SPP) was used to study remodelling behaviour in the yolk sac vasculature of 74 quail embryos and compared directly with microscopic images, demonstrating the 75 predictive power of such modelling approaches⁶.
- 76 Here, we used cell tracking data from our in vitro mosaic experiments with the level of granularity needed to parameterise an ABM of endothelial interactions in 2D monolayers 77 for the first time. By systematically varying the range of cell-cell adhesion ("cohesion"), 78 79 neighbour-displacing forces that separate adjacent cells ("extrusion"), and directed motility ("migration") in the ABM we can use Approximate Bayesian Computation with 80 81 Seguential Monte Carlo sampling (ABC-SMC) to infer the likely distribution of interaction 82 forces associated with cell adhesion, contractility, and motility to recapitulate the experimental observations. This parameter inference method is applied to EC 83 populations with knockdowns of ALK1, SMAD4 and a control to determine the difference 84 in cell mechanical interaction regimes between the different populations. This will 85 86 provide insight into forces at cell-cell junctions, which are important for maintaining 87 vascular integrity⁷.
- We found that SMAD4 knockdown cells exhibited increased motile force generation, 88 89 whereas ALK1 knockdown weakened the forces separating neighbouring cells that
- 90 normally allow cell rearrangement within the monolayer. Together, these changes
- 91
- reduced the efficiency of neighbour displacement, making it easier for cells to
- 92 intermingle without the normal checks on rearrangement.

- 93 Having investigated force transmission in 2D cell monolayers and characterised the
- 94 impact that ALK1 and SMAD4 have on them, we next ask the question of whether these

- changes can mechanistically explain AVM formation. Our ABM model of EC collective 95
- 96 dynamics during vascular remodelling was parameterised with the experimentally
- 97 derived proportional changes in cell motility, adhesion, and neighbour displacement
- 98 forces observed between control, ALK1 knockdown and SMAD4 knockdown cells. Loss
- 99 of flow and reversal of flow in remodelling networks have previously been postulated to
- be associated with shunt formation⁵. By quantifying the proportion of vessels in a 100
- network in which flow is lost or reversed over time we can determine whether the 101
- 102 changes in cell adhesion and directional migration associated with each knockdown are
- predictive of AVM formation. Our simulations indeed predict that AVM are more likely to 103
- 104 arise from the loss of either SMAD4 or ALK1, through distinct mechanisms.
- 105 Taken together, our combined experimental-computational approach describes changes
- 106 in EC force dynamics in SMAD4 and ALK1 deficient cells and predicts that deficiencies
- 107 of either will create emergent conditions favourable to AVM formation in vivo.

Results

108

109 110

111

Cell motion and intercellular force coefficients from in vitro EC mosaic

112 experiments

- Control and ALK1 knockdown cells were measured to be of similar sizes (cell width 113
- 114 15µm) while SMAD4 knockdown cells were larger (cell width 19µm). Measurements of
- cell direction of motion with respect to flow and inference of intercellular force 115
- 116 coefficients were obtained from live images from in vitro mosaic experiments of
- control/control and control/knockdown EC monolayers exposed to flow for 36 hours 117
- 118 (Fig. 1A).
- For cell mosaic experiments with control/SMAD4 knockdown, an average of 88.3 +/-119
- 4.7% cells were moving against the direction of flow, a greater proportion than the 120
- control/ALK1 knockdown experiments (68.2 +/- 6.1%) (Fig.1B). In control/control 121
- mosaic experiments an average of 42.0 +/- 18.2% moved against flow, though this 122
- proportion was found to rise as the cells were exposed to flow beyond 36 hours (see 123
- Supplementary materials, Table S1). 124
- The coefficient of cell migration force (k_{mig}) in the control/control and control/ALK1 125
- knockdown mosaic experiments was inferred to be similar in magnitude (1.35+/-0.16 126
- 127 and 1.40+/-0.14 respectively) while k_{mig} in the control/SMAD4 knockdown cells was
- found to be higher (2.92+/-0.75) (Fig. 1C). The average coefficient of cell cohesion force 128
- 129 (k_{coh}) was slightly lower in the control/ALK1 knockdown cells (0.10+/-0.03) compared to
- control/SMAD4 and control/control cells (0.14+/-0.12 and 0.19+/-0.15 respectively) (Fig.
- 130
- 131 1D). The large ranges of k_{coh} in control/SMAD4 knockdown and control/control cells
- 132 suggest that any differences in cohesion force are not significant. Control/ALK1
- 133 knockdown cells showed cell extrusion force (k_{ext}) to be consistently low (0.08+/-0.01)
- compared to control/control and control/SMAD4 knockdown cells (0.13+/-0.07 and 134
- 135 0.13+/-0.06 respectively).
- 136 From equation (1), the average work required to push two neighbouring cells apart
- 137 W_{push} (Fig. 1E) was found to be lower for both control/SMAD4 knockdown (0.045+/-
- 138 0.015) and control/ALK1(0.054+/-0.004) knockdown cells than the control/control cell
- experiments (0.094+/-0.036). In the case of control/SMAD4 knockdown this is due to 139

the high k_{mig} while in control/ALK1 knockdown this is due to the lower k_{ext} . Assuming

- cell yield stretch is constant, the average work required to pull two neighbouring cells
- together W_{pull} was found to be slightly lower in control/SMAD4 knockdown (0.005+/-
- 143 0.004) and control/ALK1 knockdown (0.008+/-0.003) than control/control cells (0.018+/-
- 144 0.015) (Fig 1G).

145

Experimental force measurements predict AVM-like behaviours in SMAD4 and

146 ALK1 knockdowns

- 147 Previous work⁵ quantifying EC behaviour in 'honeycomb' networks of vessels simulating
- vascular remodelling found that AVM formations were associated with increases in the
- proportion of vessels with flow loss and flow reversal. In these models, flow
- disturbances arose due to the accumulation of ECs which blocked or diverted blood flow.
- 151 It was also shown that varying the magnitude of W pull affects the proportion of vessels
- 152 with both flow loss and flow reversal in a manner dependent upon the proportion of
- 153 cells moving against the direction of blood flow. Here, the experimentally derived
- intercellular force parameters (see Table 1) and cell direction of motion with respect to
- 155 flow from *in vitro* experiments were applied to simulated honeycomb vessel networks
- and changes in vessels with flow drop out and flow reversal were recorded. Proportions
- of cells moving with or against flow changed significantly over time for control only cells
- populations in in vitro experiments (see Supplementary Materials Table S1). Values of
- proportional cell direction were therefore taken from results after 60 hours in flow.
- rather than the 36 hours recorded above, to allow cell motion to reach an equilibrium.
- During the first 36 hours of exposure to flow, simulations of control only cells had more
- 162 vessels with flow dropout than both control/SMAD4 knockdown and control/ALK1
- knockdown simulations (Fig. 2A). After 36 hours, the number of vessels with flow
- dropout in control/SMAD4 knockdown cell simulations increased to greater than control
- only cells (28.6+/-9.7% and 19.9+/-12.9% respectively at 120 hours in flow). Flow
- dropout in the control/ALK1 knockdown cell simulations remained lower until 60 hours
- in flow after which it increased until it was a similar proportion to control/control cells.
- The proportion of cells with reversal of flow direction compared to the initial state was
- greater in control/SMAD4 knockdown cell simulations than control simulations over the
- first 96 hours of simulation (Fig. 2B) after which it decreased to a similar proportion as
- 171 control cells. Vessels in control/ALK1 knockdown cell simulations initially had a similar
- proportion of reversed flow to control cells though this proportion increased gradually
- over time while reversed flow in control cell vessels plateaued leading to a greater
- proportion of reversed flow in control/ALK1 knockdown cell simulations later on (6.5+/-
- 3.7% in control/ALK1 knockdown and 4.2+/-3.4% in control at 120 hours in flow).
- 176 Examples of changes in vessel geometry and flow between control and knockdown
- 177 simulations after 120 hours are shown in Figures 2 C-E. The average diameter of
- perfused vessels was found to be significantly larger in both control/SMAD4
- knockdown (p=0.007) and control/ALK1 (p=0.024) simulations with control/SMAD4
- 180 producing the largest average increase (Fig 2F). Vessel diameters were also found to be
- less uniformly distributed in networks with ALK1 or SMAD4 knockdown cells than
- control cells alone with the coefficient of variation in vessel diameter significantly larger

in control/SMAD4 (p=0.012) and control/ALK1 (p=0.04). Progression of simulated 183 average vessel diameter and coefficient of variation in vessel diameter over time are 184 shown in Supplementary Materials Fig S1A-B. 185

Discussion

186

187

192

188 HHT is characterised by vascular abnormalities in the form of AVMs. Disruption of the BMP 9/10 signalling pathway has been linked to AVM formation in both humans¹⁰ and 189 190 mice¹¹, but the specific contributions of individual pathway components, and the 191 mechanisms by which they act, remain unclear. Here, we combine in vitro mosaic endothelial cell cultures with agent-based simulations of collective cell dynamics to dissect the distinct roles of the receptor ALK1 and the transcription factor SMAD4, both 193 194 of which have been associated with AVM development.

- 195 By calibrating cell-cell interaction parameters in the ABM using experimental observations, we show that both ALK1 and SMAD4 knockdowns influence 196
- 197 neighbouring wild-type cells, altering the physical interactions that govern collective EC
- 198 behaviour. Notably, SMAD4 knockdown cells exhibit enhanced motile force generation,
- while ALK1 knockdowns reduce the forces that normally allow endothelial cells to 199
- 200 separate and rearrange within the layer. These represent two mechanistically distinct
- 201 modes by which intercellular force balance is perturbed.
- Incorporating these altered forces into simulations of vascular remodelling, we predict 202
- 203 that both knockdowns increase the likelihood of AVM formation, but via divergent
- mechanisms. SMAD4 knockdown populations were highly polarised against flow and 204
- 205 displayed elevated migration velocities, which, over time, are predicted to cause local
- 206 cell aggregation and AVM formation. These predictions are supported by our simulation
- 207 findings, where flow dropout increases significantly in SMAD4-deficient vascular
- 208 networks over time. The characteristic phenotype of increased diameter of a single
- 209 vessel in SMAD4 knockdown populations predicted by our simulated vessels matches
- in vivo observations of mouse retinal vasculature upon knockout of SMAD412.13. 210
- 211 In contrast, ALK1 knockdowns displayed less consistent polarity, with a higher
- 212 proportion of cells migrating against one another. However, the weakened neighbour-
- separating forces in these cells allowed easier cell passage and prevented vessel 213
- 214 blockage, despite the emergence of flow reversals.
- These observations align with previous simulation studies⁵ that show imbalances 215
- 216 between cell-cell adhesion and displacement forces can disrupt EC rearrangements
- 217 and promote shunting or vessel occlusion. Importantly, our simulations predict
- 218 that SMAD4 loss leads to an imbalance between motility and adhesion that drives
- 219 strongly aligned migration, while ALK1 loss disrupts polarity with subtler mechanical
- 220 consequences, resulting in divergent vascular phenotypes.
- From cell mosaic experiments we found that knockdowns of either gene influenced the 221
- 222 polarity of neighbouring wild-type cells, causing faster collective alignment relative to
- 223 control populations. This suggests that local signalling or mechanical feedback
- 224 between mutant and wild-type ECs may amplify migratory biases and further
- 225 destabilise vessel structure.

- We acknowledge limitations in our modelling framework. Our agent-based simulations
- do not currently account for additional regulators of EC dynamics, such as angiogenic
- 228 sprouting in response to VEGF gradients or shear-stress heterogeneity. The simplified
- vascular-network geometries also limit topological plasticity, including angiogenesis
- beyond the original geometry. Moreover, other components of the vascular environment
- known to influence EC behaviour and vessel stability, such as the basement membrane
- and mural-cell interactions, are not included in our numerical model. Nonetheless, this
- 233 reduced complexity enables mechanistic dissection of specific force perturbations and
- 234 provides a computationally efficient platform for testing candidate hypotheses related
- 235 to AVM formation.
- 236 In summary, our combined experimental and computational results indicate that ALK1
- and SMAD4 knockdowns lead to AVM-prone vascular phenotypes via distinct
- perturbations in endothelial force balance. SMAD4 deficiency drives EC aggregation
- and vessel obstruction through excessive motility and polarised migration, while ALK1
- loss promotes flow reversal through impaired polarity and reduced capacity for
- 241 neighbour displacement. Together, these findings demonstrate how distinct genetic
- 242 mutations converge on vascular pathology through disruptions in collective cell
- 243 dynamics, providing a framework for linking molecular signalling defects to emergent
- 244 biomechanical behaviours.

Materials and Methods

Cell Culture

245246

247

265

- 248 HUVECs were commercially obtained and cultured in MV2 media (PromoCell). Cells
- 249 were cultured in gelatinized cell culture flasks and used at passages 2-4. Cells were
- 250 kept at 37 degrees in a 5% CO₂ humidity incubator. Knockdown of target genes was
- achieved by transfecting HUVECs at 60-70% confluence using 10nM siRNA for siCTRL
- 252 (Qiagen AllStars negative control), siSMAD4 (FlexiTube GeneSolution for SMAD4,
- 253 Qiagen) or siALK1 (FlexiTube GeneSolution for ALK1, Qiagen) and RNAiMax
- 254 transfection reagent (Thermofisher) diluted in antibiotic free transfection media
- 255 (EBM2+OptiMEM) for 5h. Cells were labelled the next day with CellTracker Green or
- 256 Red (Thermofisher) prior to seeding into flow slides. Briefly, cells were washed once
- 257 with sterile PBS, and incubated for 45 minutes at 37C with 1:5000 CellTracker diluted in
- 258 EBM2 media to a final concentration of 2nM. At the end of the incubation, labelling
- 259 media was aspirated and cells were washed 3 times with MV2 media. Cells were then
- 260 harvested and mixed at 1:1 ratio, and seeded onto gelatinized 0.4 Luer slides (Ibidi) at a
- concentration of 2 million cells/ml. Slides were incubated overnight to allow cells to
- attach and form a monolayer. Further details of the cell culture methodology used are
- described in Oppenheim et al. (2025)¹³ as well as results of qPCR and Western blot
- assays illustrating the degree to which siRNAs reduce protein expression.

Shear stress experiments

- 266 MV2 growth media was aspirated from slides and replaced with CO₂ independent
- media (Promocell basal media without phenol-red and without sodium bicarbonate,
- supplemented with MV2 supplement kit, B-glycerolphosphate at a final concentration of
- 4.32ug/ul and sodium bicarbonate at a final concentration of 0.0075%). Slides were

- 270 connected to fluidic units (Ibidi) and placed within the incubation chamber of the
- 271 microscope. Shear stress of 0.6 Pa was applied 1 hour after start of imaging for
- 272 approximately 2.5 days.

Microscopy

273

283

293

- 274 Slides were imaged in pairs using a Zeiss 980 Confocal inverted microscope with a 20x
- air objective. Imaging setup included 2 selected positions in the middle of every slide;
- each position was set up with 3x3 tiles and 5-slice Z-stack. Two acquisition green and
- 277 red channels were set up using the 488 and 561 lasers, respectively. To avoid photo-
- bleaching, laser intensity was minimized, and signal detection was enhanced by
- enlarging the pinhole size to 4 AU. Live imaging was defined as a time series of 500
- 280 cycles with 7.5-minute intervals. Imaging started one hour prior to shear stress
- application. CZI files were exported to Fiji. Maximum intensity projection was applied to
- each position, and files were saved in TIF format.

Image segmentation

- Live images of fluorescent cells were segmented after 36 hours of exposure to
- unidirectional flow. Cells were segmented using Labkit for ImageJ⁸. Segmented images
- were manually inspected to add centroids of unlabelled cells and correct mislabelled
- cells. Segmented cells were tracked over 4 subsequent frames (30 minutes total) using
- 288 Trackmate for ImageJ. Cell fluorescence colour and centroid position were recorded for
- 289 each timeframe and distance moved parallel and perpendicular to flow was measured
- between the first and last frames. Cells were labelled as migrating with or against flow
- depending upon whether the component of cell displacement parallel to flow was
- 292 positive or negative.

Agent-based model

- The ABM is described in detail in Edgar et al. ECs are represented as agents consisting
- of nested ellipses. EC agents migrate in the direction of polarisation at a speed
- determined by the coefficient of migration force (k_{mig}). If neighbouring EC agents are
- 297 positioned such that their outer ellipses are overlapping, they experience a cohesive
- 298 force representing cell-cell tension determined by the coefficient of cohesion (kcoh) and
- scaled magnitude of the overlap. If EC agents are positioned such that their inner
- 300 ellipses overlap, they transmit an extrusive force representing cell-cell compression
- determined by the coefficient of extrusion (k_{ext}). Following the initial movement of cells at
- each timestep, the forces are then recalculated, and cells are intercalated iteratively
- until all forces are in equilibrium. The new cell positions are given as an output.
- 304 Since the effect of cell forces on vessel dynamics is dependent upon the relationship
- between extrusion or cohesion forces and migration force, the force coefficients can be
- 306 combined as ratios to represent the work required to elicit cell behaviours. The work
- required to push two adjacent cells together is given by:

$$W_{push}^* = \frac{k_{ext}}{k_{mig}} \tag{1}$$

While the work required to pull two adjacent cells apart is given by:

310
$$W_{pull}^* = \frac{k_{coh}|1-\Gamma|^3}{k_{mig}}$$
 (2)

- Where Γ is the yield stretch, the maximum stretch ratio of a cell before junction
- 312 connections are lost. Γ was set to a constant value of 1.5 throughout. The ABM
- contains a 'flow sensitivity' parameter regulating the time taken for cells to become
- polarised with flow. In this study, it was also assumed that after 36 hours in flow all cells
- would begin polarised in parallel with the direction of flow.
- 316 For inference of intercellular force coefficients from in vitro cell experiment, the
- 317 geometrical constraints of the ABM were set to a flat plate with dimensions dependent
- upon the size of the experimental image for which they are simulating. Cells were
- seeded in simulations depending on the location of their centroids measured from the
- 320 corresponding in vitro experiment. Cell length was taken from an average of
- measurements of segmented in vitro cells. Cells leaving one edge of the geometry enter
- 322 on the opposite edge.

309

- For simulations of vascular networks, cells were seeded into an idealised 'honeycomb'
- 324 plexus of bifurcating vessels⁵. Individual vessels were formed from a 50 μm length with
- 5 discrete cylindrical segments and each segment initiated with 4 ECs of length 10 μm
- and width 5 μm . Vessel radius changes depending upon the flux of cells into and out of
- a lumen segment. Pressurised fluid is simulated within the vessel lumens, with pressure
- 328 stored at nodes between luminal segments. Flow at inlets and outlets is at constant
- 329 pressure but changes dynamically within the network with changes in vessel radius. A
- flow magnitude of less than $10^{-5} \mu l/hr$ within a vessel is defined as "no flow" and
- 331 recorded as flow drop out.

Approximate Bayesian Inference

- Values of k_{mig} , k_{coh} and k_{ext} are inferred from experimental measurements of cell
- displacement using approximate Bayesian computation with a sequential Monte Carlo
- sampling method (ABC-SMC)⁹. The ABM is run with input parameter values sampled
- from a prior distribution within a reasonable range (we apply uniform distributions with
- range 0-1 for k_{coh} and k_{ext} and 0-5 for k_{mig}). The vertical (perpendicular to flow) and
- 338 horizontal (parallel to flow) distances between simulated cell locations as outputs from
- 339 the ABM and those measured from in vitro experiments is calculated and used to
- 340 generate a loss function to determine the accuracy of that simulation. ABC-SMC runs
- multiple simulations with varying input parameter values and selects samples from
- which the loss function is below a threshold (ε) to build a probability distribution for
- 343 likely parameter values. ε is systematically decreased, and so, if a solution is possible,
- the probability distribution will converge towards the most likely values for each of the
- 345 parameters.
- The loss function for comparison of experimental and simulated cell displacement is as
- 347 follows:

$$LF = \sqrt{\tilde{X}^2 + \tilde{Y}^2} \tag{3}$$

Where 349 $\tilde{X} = Median(x_{expt,i} - x_{sim,i}, ..., x_{expt,n} - x_{sim,n}),$ 350 $\tilde{Y} = Median(y_{exnt,i} - y_{sim,i}, ..., y_{exnt,n} - y_{sim,n})$ and 351 $x_{expt,i}$, $y_{expt,i}$ are experimentally measured centroid coordinates of cell i in the 352 directions parallel and perpendicular to flow respectively and $x_{sim,i}$. $y_{sim,i}$ are simulated 353 354 centroid coordinates of cell i in the directions parallel and perpendicular to flow respectively. 355 356 Application of flat plate force coefficients to an idealised vascular plexus 357 Once k_{min} , k_{coh} and k_{ext} have been inferred from in vitro experiments on flat plates, the relative differences in their values are applied as parameter inputs to the ABM with the 358 simplified 'honeycomb' vascular network geometry. In previous simulations of ECs in a 359 vascular plexus⁵, intercellular force coefficient values for k_{mig} =3, k_{coh} =1/3 and k_{ext} =3 360 were found to generate stable networks, free from adverse vascular remodelling and 361 with cell migration speeds similar to those found in vivo. Intercellular force coefficients 362 363 for control cells were therefore set to these values. Values for intercellular force coefficients in vessel networks with control and knockdown cells were calculated using 364 365 the following equation: $k_{\alpha \ vessels} = \frac{k_{\alpha \ control \ vessels} k_{\alpha \ cells}}{k_{\alpha \ control \ cells}}$ 366 (4)Where $k_{\alpha_control_vessels}$ and $k_{\alpha_vessels}$ are force coefficients for vascular plexus 367 simulations for control and control/knockdown experiments respectively and 368 $k_{\alpha \ control \ cells}$ and $k_{\alpha \ cells}$ are force coefficients inferred from in vitro experiments for 369 370 control and control/knockdown experiments respectively. Edgar et al. also found that the formation of shunts in simulated vessel networks 371 372 analogous to AVM was associated with loss of perfusion and/or reversal of flow in vessels and so measurement of perfusion loss and flow reversal in vessels are used 373 here as indicators of AVM formation. To assess AVM-like vascular remodelling, the 374 375 mean of all vessel diameters in perfused vessels was recorded as well as the coefficient 376 of variation of vessel diameters (standard deviation in vessel diameter/mean vessel 377 diameter), an indicator of uniformity of vessel width. 378 A set of 21 random seed numbers were generated and used to randomise the starting positions for cells within the simulated vascular plexus. Each starting position was used 379 to simulate cells with cell force coefficients and cell direction of motion matching 380 control, ALK1 knockdown and SMAD4 knockdown ECs. 381 Statistics and code availability 382 Results for measured and inferred values from in vitro cell experiments are shown +/- 1 383

standard deviation from the mean. Features of ABM vessel network simulations are

- shown +/- 95% confidence interval. Two-sample t-tests were used to assess 385
- significance of differences in vessel. Statistical analysis was conducted in Matlab. 386
- 387 The agent-based modelling code, together with scripts linking the ABM to pyABC and 388
 - example tracking datasets, is available at https://github.com/dhardma2/EC_ABM

Acknowledgments

We thank Lowell Edgar for developing the original version of the agent-based modelling scripts used and adapted in this study.

References

389 390

391 392

393

394

395

396

397

398

399 400

401

402

403

404 405

406

407

408

409 410

411

412

413

414

415 416

417 418

419

420

421

422

423 424

- 1. J. L. Lucitti et al., Vascular remodeling of the mouse yolk sac requires hemodynamic force. Development 134, 3317-3326 (2007).
- 2. C. A. Franco et al., Dynamic Endothelial Cell Rearrangements Drive Developmental Vessel Regression. PLoS Biol 13, e1002125 (2015).
- 3. D. W. Johnson et al., Mutations in the activin receptor-like kinase 1 gene in hereditary haemorrhagic telangiectasia type 2. Nat Genet 13, 189-195 (1996).
- 4. R. Ola et al. SMAD4 prevents flow induced arterial-venous malformations by inhibiting Casein Kinase 2. Circulation 138, 2379 (2018).
- 5. L. T. Edgar et al., Traffic Patterns of the Migrating Endothelium: How Force Transmission Regulates Vascular Malformation and Functional Shunting During Angiogenic Remodelling. Frontiers in Cell and Developmental Biology 10, 1 (2022).
- 6. A. Tabibian, S. Ghaffari, D. A. Vargas, H. Van Oosterwyck, E. A. V. Jones, Simulating flow induced migration in vascular remodelling. PLoS Comput Biol 16, (2020).
- 7. A. Szymborska, H. Gerhardt, Hold Me, but Not Too Tight-Endothelial Cell-Cell Junctions in Angiogenesis. Cold Spring Harb Perspect Biol 10, (2018).
- 8. M. Arzt et al., LABKIT: Labeling and Segmentation Toolkit for Big Image Data. Front Comput Sci 4, (2022).
- 9. D. Hardman, K. Hennig, E. R. Gomes, W. Roman, M. O. Bernabeu, An in vitro agentbased modelling approach to optimization of culture medium for generating muscle cells. J R Soc Interface 21, (2024).
- 10. H. Choi et al., BMP10 functions independently from BMP9 for the development of a proper arteriovenous network. Angiogenesis 26, 167–186 (2023).
- 11. S. Ruiz et al., A mouse model of hereditary hemorrhagic telangiectasia generated by transmammary-delivered immunoblocking of BMP9 and BMP10. Sci Rep 5, (2016).
- 12. A. M. Crist et al., Vascular deficiency of Smad4 causes arteriovenous malformations: a mouse model of Hereditary Hemorrhagic Telangiectasia. Angiogenesis 21 363-380 (2018)
- 13. O. Oppenheim et al., Gene-specific endothelial programs drive AVM pathogenesis in SMAD4 and ALK1 loss-of-function. bioRxiv, doi:10.1101/2025.01.03.631070, posted October 18, 2025 [Preprint].

Figures and Tables

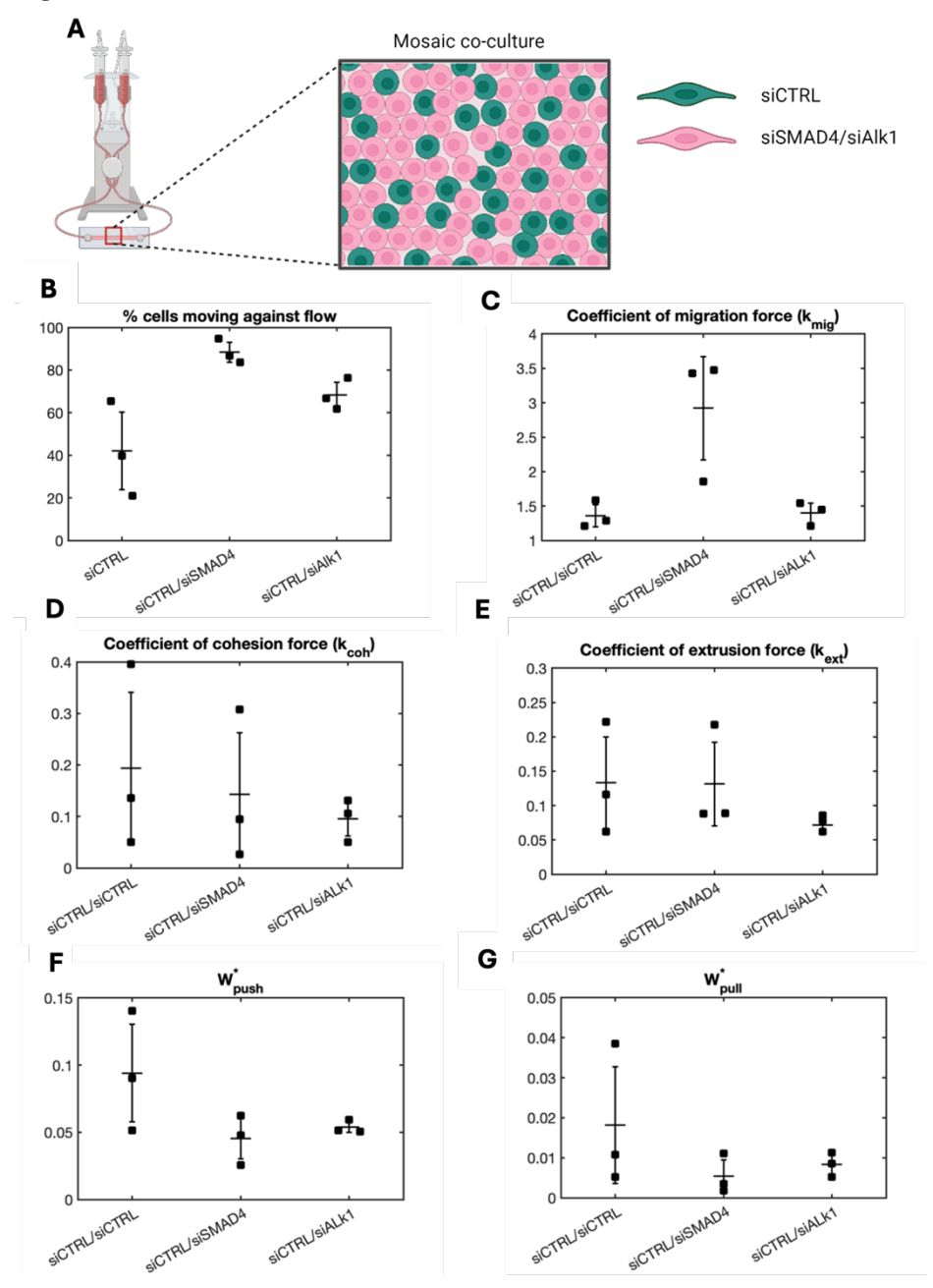


Figure 1. Figure 1: **Measurements of cell direction of motion and inferred intercellular force.** (**A**) Sketch of fluid pump system (left) and illustration of stained endothelial cell mosaic, siCTRL in green and siALK1 cells in magenta (right). (**B**) Percentage of cells moving against the direction of flow (**C-E**) Inferred coefficients of intercellular forces. (**F**) Work required to push neighbouring cells together (W^*_{push}). (**G**) Work required to pull neighbouring cells together (W^*_{pull}). Data for plots B-G obtained from cells after 36 hours of exposure to 6 dyne/cm² unidirectional flow (mean +/- 1 standard deviation)

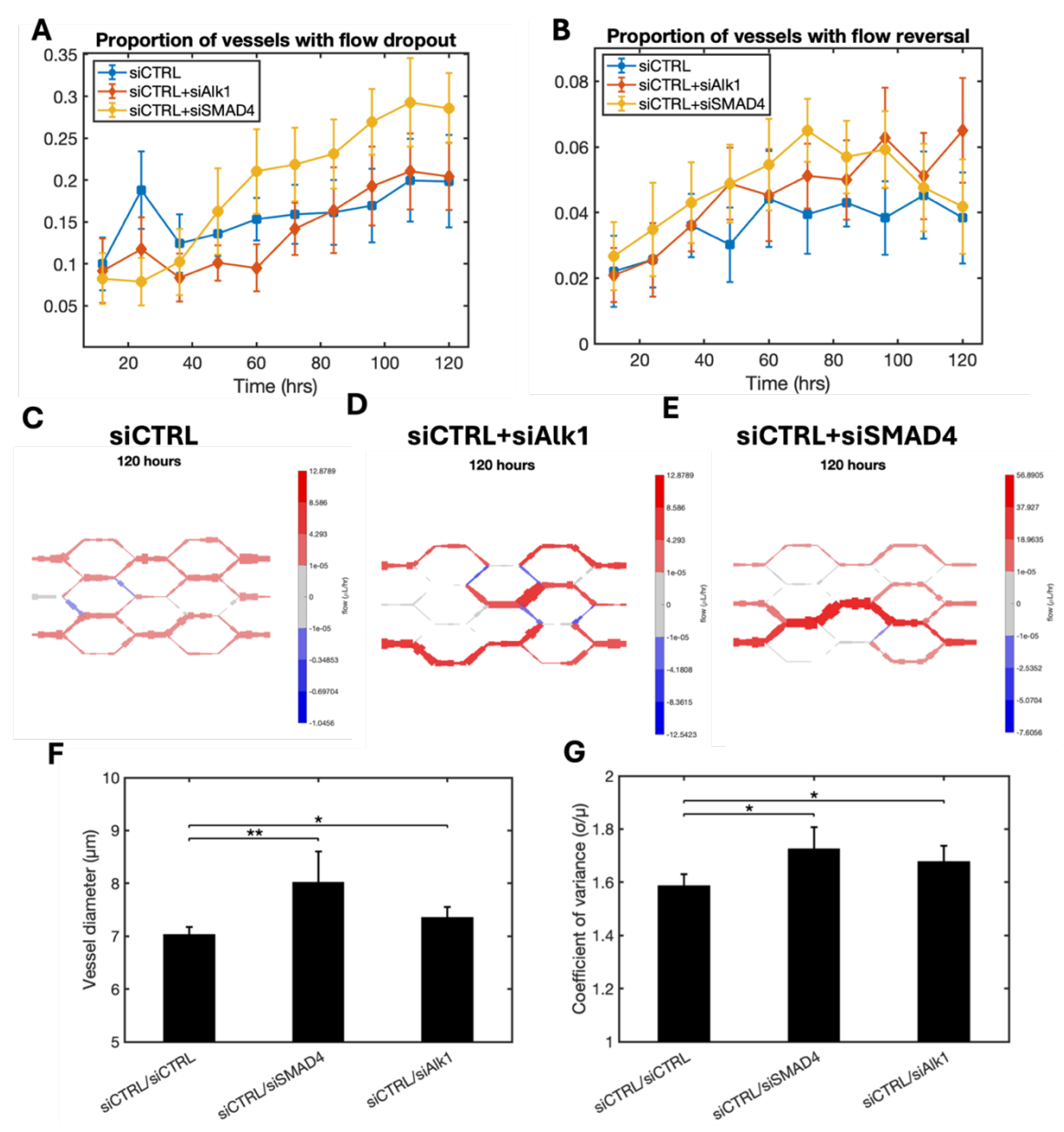


Figure 2. Figure 2: **Comparison of AVM associated features in honeycomb vessel networks of endothelial cells.** (**A**) Proportion of vessel segments with magnitude of flow less than 10^{-5} uL/hr. (**B**) Proportion of vessel segments with flow reversal compared to original flow direction (n=21, mean +/- 95% CI). (**C-E**) Example images of simulated blood flow magnitude and direction and vessel thickness in vessel networks after 120 hours of development with endothelial cell force coefficients proportional to those inferred from in vitro experiments. (**F**) Mean vessel diameter in perfused vessel segments after 120 hours of development. (**G**) Mean coefficient of variation in perfused vessel segments after 120 hours of development. Plots A, B, F and G show mean +/- 95% CI with n = 21.

Experiment	Force coefficients from <i>in</i> vitro measurement			Force coefficients for Vascular networks		
	k _{mig,}	K _{coh}	K _{ext}	K _{mig,}	K _{coh}	K _{ext}
siCTRL/siCTRL	1.36	0.194	0.133	3	0.333	3
siCTRL/siALK1	1.4	0.096	0.072	3.09	0.165	1.623
siCTRL/siSMAD4	2.92	0.143	0.131	6.45	0.246	2.955

Table 1. Intercellular force coefficients inferred from in vitro experiments and converted to vascular networks using equation (4).